Pattern formation in a reaction-diffusion system with space-dependent feed rate

Theodore Kolokolnkov and Juncheng Wei

Abstract. We consider a standard reaction-diffusion system (the Schnakenberg model) that generates localized spike patterns. Our goal is to characterize the distribution of spikes in space and their heights for any spatially-dependent feed rate $A(x)$. In the limit of many spikes, this leads to a fully coupled nonlocal problem for spike locations and their heights. A key feature of the resulting problem is that it is necessary to estimate the difference between its continuum limit and the discrete algebraic system to derive the effective spike density. For a sufficiently large feed rate, we find that the effective spike density scales like $A^{2/3}(x)$ whereas the spike weights scale like $A^{1/3}(x)$. We derive asymptotic bounds for existence of N spikes. As the feed rate is increased, new spikes are created through self-replication whereas the spikes are destroyed as the feed rate is decreased. The thresholds for both spike creation and spike death are computed asymptotically. We also demonstrate the existnence of complex dynamics when the feed rate is sufficiently variable in space. For a certain parameter range which we characterize asymptotically, new spikes are continously created in the regions of high feed rate, travel towards regions of lower feed rate and are destroyed there. Such "creation-destruction loop" is only possible in the presence of the heterogenuity.

1. INTRODUCTION

Reaction-diffusion PDE's are ubiquitous as models of pattern formation in a variety of biological and social systems. Some prominent examples include: animal skin patterns [1–3]; vortex lattices in Bose-Einstein condensates [4, 5]; patterns in chemical reactions [6–8]; crime hot-spots in a model of residential burglaries [9–12]; and vegetation patches in arid environments [13–16] A common feature of many of these systems is the presence of localized patterns such as spots, stripes etc. There is a very large literature about the formation and stability of these patterns, especially within homogeneous environments. We refer the reader to books [17–21] and references therein.

While initial pattern formation and various instabilities are by now well studied, much less is known about distribution of resulting patterns, especially – as is often the case in nature – if there are spatial inhomogenuities. For example, vortex crystals in Bose Einstein condensates form in the presence of a rotating confining trap, which is modelled by Gross-Pitaevskii equation with a space-dependent potential [22]. The condensates are not uniformly distributed, but have a higher density near the center of the trap [23–25]. Animal skin patterns are also highly dependent on the location within the animal, since the thickness, curvature and growth of the skin is nonuniform and has a large effect on the resulting patterns [26–31]. Similarly, the distribution of the vegetation patches is highly dependent on the amount of precipitation and slope gradients which vary in space and time [16, 32, 33].

In this paper we study the spot distribution and stability for a one-dimensional reaction-diffusion model with a space-dependent feed rate. For concreteness, we concentrate on the well-studied Schnakenberg model [34–36] but we anticipate these techniques can be extended to other settings. We consider the following limiting scaling of the Schnakenberg model,

$$\begin{cases} \varepsilon^2 u_t = \varepsilon^2 u_{xx} - u + u^2 v, & x \in (-L, L) \\ 0 = v_{xx} + a_0 A(x) - \dfrac{u^2 v}{\varepsilon}, & x \in (-L, L) \\ \quad u_x = 0 = v_x \text{ at } x = \pm L \end{cases} \tag{1.1}$$

These equations model the following process: a fast-diffusing substrate v is consumed by a slowly diffusing activator u, which decays with time. The substrate is being pumped into the system at some space-dependent feed rate $a_0 A(x)$. The constant a_0 represents the overall feed strength and we will use it as the control parameter. The reaction kinetics for u and v occur at different scales: u reacts much slower than v, so that v is effectively slave to u. This model is also a limiting case of the Klausmeyer model of vegetation (where u represents plant density, v represents water concentration in soil, $a_0 A(x)$ is the precipitation rate, and v_{xx} is replaced by $v_{xx} + cv_x - dv$) as well as the Gray-Scott model (where v_{xx} is replaced by $v_{xx} - dv$). As such, the Schnakenberg model is among the simplest prototypical reaction-diffusion models.

In the limit $\varepsilon \to 0$, the system (1.1) is well known to to generate patterns consisting of spots (or spikes) [28, 35, 36]. In the case of a constant feed rate $A(x) = 1$, the equilibrium consists of a sequence of equally-spaced spikes as illustrated in Figure 3. On the other hand, when $A(x)$ is spatially dependent, the spike spacing is non-uniform, as shown in Figure 1(a). The goal of this paper is to describe the density distribution of spikes and their stability in this situation.
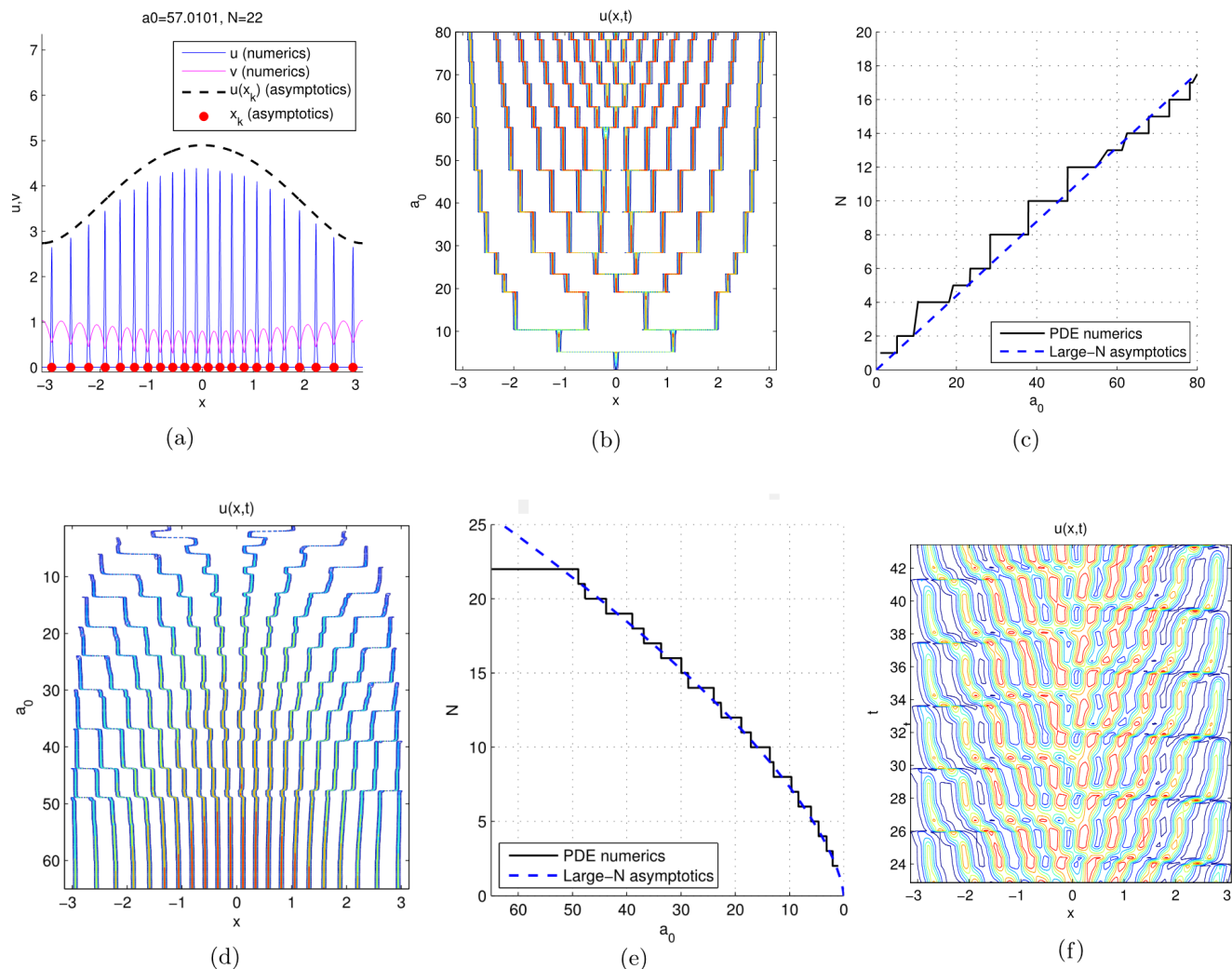
FIG. 1. (a) Stable equilibrium configuration having 22 spikes. Red dots and dashed line are the theoretical prediction for the density and spike heights as given in Main Result 2.2. Here, $A(x) = 1 + 0.5 \cos(x)$, $L = \pi$, $\varepsilon = 0.007$ with a_0 as shown. Note that the steady state is non-uniform, unlike the case of constant a (see figure 3). (b) Illustration of spike creation. Full numerical simulation of (1.1) where a_0 is gradually increased according to the formula $a_0 = 1 + 0.08t$; other parameters are as in (a). New spikes are created through self-replication near the origin where $a(x)$ has its maximum. (c) The number of spots as a function of a_0. Solid stair line corresponds to the observed number of spots from the numerical simulation in (a). Dashed line is the theoretical prediction $a_0 = a_{0,split}$ given in (3.27). (d) Illustration of spike destruction. As in (b) except that a_0 is very gradually decreasing according to the formula $a0 = 120 - 0.08t$. Note that spikes are destroyed near $x \sim \pm\pi$. (e) The number of spots as a function of a_0. Solid stair curve corresponds to the observed number of spots from the numerical simulation in (a). Dashed line is the theoretical prediction $a_0 = a_{0,coarse}$ given in (3.27). (f) Creation-destruction loop with $A(x) = 1 + 0.5 \cos(x), a_0 = 20, \varepsilon = 0.05$. New spikes are created near the center and are destroyed near the edges.

We now illustrate our main results, refer to Figure 1. There, we take $A(x) = 1 + 0.5 \cos(x)$ with $L = \pi$ and either decrease or increase a_0 very slowly. For a fixed a_0 and fixed number of spikes N as illustrated in Figure 1(a), our theory (see Main Result 2.2 below) yields both the effective spike density as well as the envelope for spike heights. Note that the spike density is not uniform – it is higher at the center than boundaries – and the asymptotics recover the effective spike density very well. As a_0 is increased, new spikes are created through self-replication near the center (where $A(x)$ is at a maximum) – see Figure 1(b,c). On the other hand as a_0 is decreased, spikes are destroyed near the boundary (where $A(x)$ is at a minimum) as a result of competition or coarsening instability as shown in Figure 1(d,e). In Main Result 3.4 we show that N spikes are stable if and only if the feed strength a_0 lies within the following range,

$$\alpha N^{3/2} < a_0 < \beta N \varepsilon^{-1/2}, \quad \alpha = 0.504, \quad \beta = 0.38097. \tag{1.2}$$

Moreover, spike destruction occurs when a_0 is decreased below the curve $a_0 = \alpha N^{3/2}$ (dashed curve in Figure 1(e) and spike creation occurs when a_0 is increased above the line $a_0 = \beta N \varepsilon^{-1/2}$ (dashed line in Figure 1(c)).

The two boundaries $a_0 = \alpha N^{3/2}$ and $a_0 = \beta N \varepsilon^{-1/2}$ in (1.2) intersect when $a_0 = a_{0,\max} \equiv \beta^3/\alpha^2 \varepsilon^{-3/2}$, and there is no stable spiky steady state that exists for $a_0 > a_{0,\max}$. However for value of a_0 just above $a_{0,\max}$, very complex dynamics are observed as shown in Figure 1(f): new spikes are continually being created near the center, then move towards the boundaries and are destroyed there, resulting an infinite "creation-destruction loop". In Figure 1(f) we took $\varepsilon = 0.05$ so that $a_{0,\max} = 19.469$, whereas $a_0 = 20$ is taken just above $a_{0,\max}$ (numerical simulations confirm that no such dynamics occur if $a_0 = 19$). Such a complex dynamical loop is only possible for an inhomogeneous feed rate, since the place of destruction must differ from the place of creation. We remark that this phenomenon was also previously reported in [28], and seems to be commonplace in reaction-diffusion systems with varying parameters.

The summary of the paper is as follows. The equilibrium spike density is derived in §2. Stability is derived in §3. We conclude with some discussions and open problems in §4.

2. SPIKE DENSITY

The starting point for computing spike density and stability is to derive the reduced dynamics for spike centers. By now, this is a relatively standard asymptotic computation, see for example [37]. For completeness, we include a self-contained derivation of spike dynamics in Appendix A. We summarize it as follows.

Proposition 2.1. *Consider the Schankenberg system (1.1). Assume that $A(x)$ is even on interval $[-L, L]$. Define $P(x)$ and b by*

$$P''(x) = A(x) \quad with \quad P'(0) = 0; \qquad b \equiv 6N^3/a_0^2. \tag{2.3}$$

Assume $\varepsilon N \ll 1$. The dynamics of N spikes are asymptotically described by ODE system

$$\frac{dx_k}{dt}\frac{S_k}{18N} = \frac{1}{N}\sum_{\substack{j=1\ldots N \\ j \neq k}} \frac{S_j}{2}\frac{x_k - x_j}{|x_k - x_j|} - P'(x_k) \tag{2.4a}$$

subject to $N+1$ algebraic constraints

$$\frac{b}{N^2}\frac{1}{S_k} = \frac{1}{N}\sum_{j=1}^{N} S_j \frac{|x_k - x_j|}{2} - P(x_k) + c, \quad k = 1\ldots N; \tag{2.4b}$$

$$\frac{1}{N}\sum_{j=1}^{N} S_j = \int_{-L}^{L} A(x)dx. \tag{2.4c}$$

Near x_k, the quasi-steady state is approximated by

$$u(x) \sim \mathrm{sech}^2\left(\frac{x - x_k}{2\varepsilon}\right)\frac{S_k}{4N}, \quad v(x) \sim \frac{6N}{S_k}, \quad |x - x_k| \ll 1. \tag{2.5}$$

The next step is to construct a continuum-limit approximation for spike density. Setting $\frac{dx_k}{dt}$ to zero in (2.4a) we obtain the steady state equations

$$0 = \frac{1}{N}\sum_{j \neq k} \frac{S_j}{2}\frac{x_k - x_j}{|x_k - x_j|} - P'(x_k), \tag{2.6a}$$

$$\frac{b}{S_k}\frac{1}{N^2} = \frac{1}{N}\sum_{j} S_j \frac{|x_k - x_j|}{2} - P(x_k) + C, \quad \frac{1}{N}\sum S_j = 2P'(L). \tag{2.6b}$$

A posteriori analysis shows that N spikes are *unstable* if $b \gg 1$ (in the limit of large N), so that the relevant regime to consider is when $b = O(1)$.

To study the large-N limit, we define the *spike density* $\rho(x)$ to be a density distribution function for spikes, that is, for any $a, b \in [-L, L]$ we define $\rho(x)$ to be

$$\int_{a}^{b} \rho(x)dx \sim \frac{\# \text{ of spikes in the interval } [a, b]}{N}. \tag{2.7}$$

An alternative definition is to define

$$\rho(x) = \frac{1}{N} \sum \delta\left(x - x_j\right).$$

In the large-N limit, we consider the spike locations x_j to be a continuous function $x_j = x(j)$ from $[0, N]$ to $[-L, L]$. In terms of $x(j)$, the density may also be expressed as:

$$\rho(x(j)) = \frac{1}{Nx'(j)}, \tag{2.8a}$$

which which also gives a way to compute the effective density given a sequence of spike positions. We also define the strength function $S(x)$ to be such that

$$S_j = S(x(j)). \tag{2.8b}$$

With these definitions, we estimate the summation terms in (2.6) using integrals. For example we have $\sum_j S_j \frac{|x_k - x_j|}{2} \approx \int S(y) \frac{|x_k - y|}{2} dy$ and so on. To leading order, the continuum limit of equations (2.6) then become

$$\int_{-L}^{L} S(y)\rho(y)\frac{1}{2}\frac{x-y}{|x-y|}dy \sim P'(x), \tag{2.9a}$$

$$\int_{-L}^{L} S(y)\rho(y)\frac{1}{2}|x-y|\,dy \sim P(x) + C. \tag{2.9b}$$

The first thing to note is that the control parameter b is *not present* in the leading order computation in (2.9). What's worse, equation (2.9a) is a direct consequence of differentiating (2.9b); thus at the leading order, there is only one equation, whereas there are two unknown functions: $S(x)$ and $\rho(x)$. Nonetheless, differentiating (2.9a) and using the fact that

$$\left(\frac{1}{2}\frac{x-y}{|x-y|}\right)_x = \left(\frac{1}{2}|x-y|\right)_{xx} = \delta(x-y),$$

this leading-order computation yields the following relationship between $S(x)$ and $\rho(x)$:

$$S(x)\rho(x) = P''(x) = A(x).$$

To make further progress in determining $S(x)$ and $\rho(x)$ requires a careful estimate for the difference between the discrete sums in (2.6) and their integral approximations. This estimate is supplied by the Euler-Maclaurin formula which we recall here. Assume that $f(n)$ is sufficiently smooth function from $[1, N]$ to $\mathbb{R}$. Then

$$\sum_{j=1}^{N} f(j) = \int_{1}^{N} f(j)dj + \frac{1}{2}\left(f(1) + f(N)\right) + \sum_{j=1}^{K} c_j \left(f^{(j)}(N) - f^{(j)}(1)\right) + R_K \tag{2.10}$$

where c_j are coefficients that are related to Bernoulli numbers and the remainder R_K depends only on higher-order derivatives of f. Here, we only need the first two coefficients:

$$c_1 = \frac{1}{12}, \quad c_2 = 0.$$

(in fact all even coefficients are zero). We now apply the Euler-Maclaurin formula to estimate the sums in (2.6). We start by estimating

$$\frac{1}{N} \sum_{j \neq k} \frac{S_j}{2} \frac{x_k - x_j}{|x_k - x_j|} = \frac{1}{N} \sum_{j=1}^{k} S(x(j)) - \frac{1}{N} \sum_{j=k}^{N} S(x(j)).$$

By changing variables $x(j) = y, \quad dj = \frac{dy}{x'(j)} = N\rho(y)dy$, we obtain

$$\frac{1}{N} \sum_{j=1}^{k} S(x(j)) = \int_{x_1}^{x_k} S\left(y\right)\rho(y)dy + \frac{1}{2N}\left(S(x_1) + S(x_k)\right) + \frac{1}{12N^2}\left(\frac{S'(x_k)}{\rho\left(x_k\right)} - \frac{S'(x_1)}{\rho(x_1)}\right) + O\left(\frac{1}{N^4}\right)$$

$$\frac{1}{N}\sum_{j=k}^{N}S(x(j)) = \int_{x_k}^{x_N} S(y)\,\rho(y)dy + \frac{1}{2N}\left(S(x_k)+S(x_N)\right) + \frac{1}{12N^2}\left(\frac{S'(x_N)}{\rho(x_N)}-\frac{S'(x_k)}{\rho(x_k)}\right) + O\left(\frac{1}{N^4}\right)$$

so that

$$\frac{1}{N}\sum_{j\neq k}S_j\frac{x_k-x_j}{|x_k-x_j|} = \int_{x_1}^{x_N} S(y)\,\rho(y)\frac{x_k-y}{|x_k-y|}dy + \frac{1}{2N}\left(S(x_1)-S(x_N)\right) + \frac{1}{12N^2}\left(\frac{2S'(x_k)}{\rho(x_k)}-\frac{S'(x_1)}{\rho(x_1)}-\frac{S'(x_N)}{\rho(x_N)}\right)$$

Assume $S(x)$ is even and that $x_1 = -x_N$. Then $S(x_1) = S(x_N)$, $\frac{S'(x_1)}{\rho(x_1)} = -\frac{S'(x_N)}{\rho(x_N)}$ and

$$\int_{x_1}^{x_N} S(y)\,\rho(y)\frac{x_k-y}{|x_k-y|}dy = \int_{-L}^{L} S(y)\,\rho(y)\frac{x_k-y}{|x_k-y|}dy + \int_{-L}^{x_1} S(y)\,\rho(y)dy - \int_{x_N}^{L} S(y)\,\rho(y)dy$$

$$= \int_{-L}^{L} S(y)\,\rho(y)\frac{x_k-y}{|x_k-y|}dy$$

so that we finally obtain

$$\frac{1}{N}\sum_{j\neq k}S_j\frac{1}{2}\frac{x_k-x_j}{|x_k-x_j|} = \int_{-L}^{L} S(y)\,\rho(y)\frac{1}{2}\frac{x_k-y}{|x_k-y|}dy + \frac{1}{N^2}\left(\frac{1}{12}\frac{S'(x_k)}{\rho(x_k)}\right) + O(N^{-4}).$$

A similar computation yields

$$\frac{1}{N}\sum_{j\neq k}S_j\frac{|x_k-x_j|}{2} = \int_{-L}^{L} S(y)\,\rho(y)\frac{|x_k-y|}{2}dy + \frac{1}{N^2}\left(-\frac{1}{12}\frac{S(x_k)}{\rho(x_k)}+C_0\right) + O(N^{-4}).$$

where C_0 is (an irrelevant) constant that depends on $S(\pm L), S'(\pm L), \rho(\pm L)$ and $\rho'(\pm L)$.

We now expand

$$S(x) = S_0(x) + \frac{1}{N^2}S_1(x) + \ldots.$$

to obtain

$$\int S_0(y)\rho(y)\frac{1}{2}\frac{x-y}{|x-y|}dy = P'(x), \quad \int S_0(y)\rho(y)\frac{1}{2}|x-y|\,dy = P(x) + C;$$

$$\int S_1(y)\rho(y)\frac{1}{2}\frac{x-y}{|x-y|}dy = -\int S_0(y)\rho(y)\frac{1}{2}\frac{x-y}{|x-y|}dy + \frac{1}{12}\frac{S_0'(x)}{\rho(x)}; \tag{2.11}$$

$$\int S_1(y)\rho(y)\frac{1}{2}|x-y|\,dy = -\int S_0(y)\rho(y)\frac{1}{2}|x-y|\,dy - \frac{1}{12}\frac{S_0(x)}{\rho(x)} + \frac{b}{S_0(x)} + C_0. \tag{2.12}$$

Upon differentiating (2.12) and substituting into (2.11) we finally obtain the following ODE that relates $S_0(x)$ and $\rho(x)$:

$$\frac{1}{12}\frac{S_0'(x)}{\rho(x)} = \frac{d}{dx}\left(-\frac{1}{12}\frac{S_0(x)}{\rho(x)}+\frac{b}{S_0(x)}\right). \tag{2.13}$$

Furthermore we have

$$S_0(x)\rho(x) = A(x); \quad \int_{-L}^{L}\rho(x)dx = 1. \tag{2.14}$$

Together, the relationships (2.13) and (2.14) fully determine $S_0(x)$ and $\rho(x)$ in terms of $A(x)$.

Solving for $\rho'(x)$ from (2.13) yields a Bernoulli ODE,

$$\rho' = \frac{2S_0'}{S_0}\rho - 12b\frac{S_0'}{S_0^3}\rho^2 \tag{2.15}$$

whose solution is readily obtained as

$$\frac{S^2}{\rho} - 12b\log(S) = C. \tag{2.16}$$

Substituting $S = A/\rho$ we find that the steady state satisfies, at leading order,

$$\frac{A^2}{\rho^3} + 12b\log(\rho/A) = C \text{ subject to } \int_{-L}^{L} \rho(x)dx = 1; \quad S\rho = A. \tag{2.17}$$

We summarize as follows.

Main Result 2.2. *Let x_j and S_j be the equilibria locations of the reduced system (2.4) with $\partial x_j/\partial t = 0$. The spike density $\rho(x)$ as defined by (2.7) is asymptotically approximated by (2.17). The spike strengths are given by $S_j = S(x_j)$.*

An important special case of the formula (2.17) is when $b \to 0$ or equivalently, $a_0 \gg O(N^{3/2})$. Then $\frac{A^2}{\rho^3} = C$ and together with $\rho S = A$, we find $\rho = C_0 A^{2/3}$, $S = C_0^{-1}A^{1/3}$, where the normalization constant C_0 is determined through $\int \rho = 1$:

$$S(x) \sim \left(\int_{-L}^{L} A^{2/3}(y)dy\right)A^{1/3}(x), \qquad \rho(x) \sim \frac{A^{2/3}(x)}{\int_{-L}^{L} A^{2/3}(y)dy}. \tag{2.18}$$

Figure 1(a) shows the direct comparison between the Main Result 2.2 and the full numerical simulations of (1.1); see also Figure 4(c). In fact, the agreement is very good even with a relatively small N (e.g. $N = 4$; not shown). There are two sources of error when comparing the asymptotics to full numerics. The first source of error is when approximating the PDE dynamics using the reduced system (2.4), which removes the ε from the PDE. This error there scales like $O(\varepsilon)$. The second source of error is made when approximating the reduced system (2.4) by its continuum limit (2.18). This error comes from to the truncation of the Euler-Maclaurin series and scales like $O(1/N^2)$. In other words, the effects of nonzero ε are captured going from the PDE (1.1) to the reduced system of Proposition 2.1 while the effects due to finite N are captured in going from the reduced system of Proposition 2.1 to the Main Result 2.2.

The equilibrium state with N spikes as given by Main Result 2.2 only exists for a restricted parameter values. This is illustrated in Figure 1. As a_0 is increased, the steady state eventually breaks because of spike replication. This is related to the effect of ε. As a_0 is decreased, the steady state eventually breaks because of overcrowding effects leading to spike destruction. This is related to the effect of N. The study of this breakdown is the topic of the next section.

3. SELF REPLICATION AND COARSENING

We begin with an examination of self-replication. Numerical simulations (c.f. Figure 1) show that self-replication is triggered if a_0 is sufficiently increased. This is a well-known phenomenon that was first identified in one dimension in [38] and was further studied in [39–43]. As explained in Appendix A, it is related to the dissapearence of the the steady state for the so-called *core problem* as a result of a fold point bifurcation. In Appendix A we show that self-replication of j-th spot is triggered when S_j is increased past $2.70\varepsilon^{-1/2}\frac{N}{a_0}$. (see (4.44)). Moreover, suppose that $a_0 \gg O(N^{3/2})$. Then from (2.18) the maximum value of S_j is given by $\max_{x\in[-L,L]} A^{1/3}(x)\left(\int_{-L}^{L} A^{2/3}(x)dx\right)$. Replacing S_j by this maximum value and replacing the inequality in (4.44) by equality yields the the following threshold.

Proposition 3.1. *(Self-replication) Let*

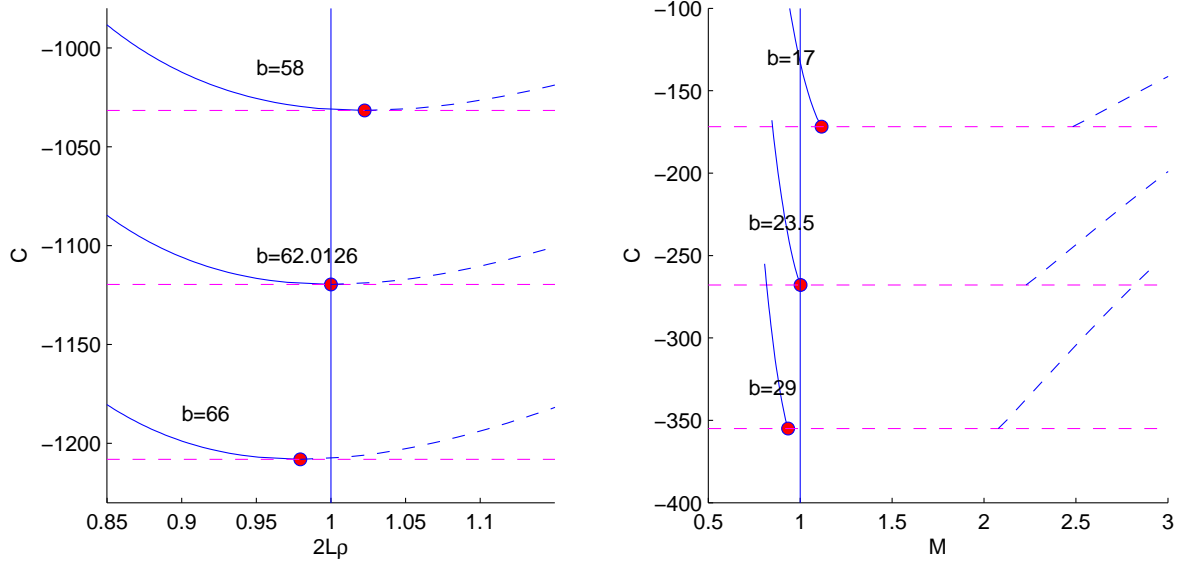$$\beta \equiv \frac{2.70}{\max\limits_{x\in[-L,L]} A^{1/3}(x)\left(\int_{-L}^{L} A^{2/3}(x)dx\right)}. \tag{3.19}$$

FIG. 2. Left: the graph of C from (2.17) as a function of total mass in the case where $A(x) = A$ is constant, for three different values of b. The threshold occurs for the value of b such that the vertical line (corresponding to total mass 1) intersects the curve precisely at the fold point. Right: The graph of C for non-constant feed rate, here $A(x) = 1 + 0.5 \cos(x)$. The red dont corresponds to $C_{\min}$. The threshold occurs when the red dot intersects the vertical line corresponding to a unit total mass.

and suppose that $N\varepsilon \ll O(1)$. Then N spikes undergo self-replication if a_0 is increased past

$$a_{0,split} \equiv \beta N \varepsilon^{-1/2}. \qquad (3.20)$$

The spike that replicates is the one closest to the maximum of $A(x)$.

The condition $N\varepsilon \ll O(1)$ is equivalent to $a_0 \gg O(N^{3/2})$ when $a_0 = O(a_{0s})$. Since the spike width is of $O(\varepsilon)$, this condition also means that the spikes are well-separated from each-other.

Figure 1(c,d) shows that the formula (3.20) is in excellent agreement with full numerical simulations.

Next we address the coarsening thresholds resulting in spike death that occur as a_0 is decreased. Consider the case of constant A first. Then (2.17) implies that ρ is also constant, so that $2L\rho = 1$. For a fixed A and b, the first equation in (2.17) defines a curve C vs. ρ as shown in Figure 2(left). The intersection of that curve with the vertical line $2L\rho = 1$ then determines the density ρ as a function of A. Note that $C(\rho)$ has a unique minimum which occurs at

$$b = \frac{A^2}{4\rho^3} \qquad (3.21)$$

with $C = C_{\min} \equiv 4b\left(1 - \log\left(4bA\right)\right)$. This fold point corresponds to a zero-eigenvalue crossing. The solution branch to the left of this minimum is stable, whereas the branch to its right is unstable. The stability threshold occurs precisely when the intersection of the vertical line $2L\rho = 1$ and the curve $C(\rho)$ happens at this minimum (refer to Figure 2). It corresponds to setting $\rho = 1/(2L)$, $C = C_{\min}$ in (2.17), which yields $b = 2A^2L^3$ or $a_0 = 3^{1/2}(N/L)^{3/2}$, with spike death occuring when a_0 is decreased below $3^{1/2}(N/L)^{3/2}$. Combining it with Proposition 3.1, we obtain the following result.

Proposition 3.2. *In the case of a constant feed rate $A(x) = 1$, of the Schankenberg model (1.1), N spikes are stable provided that*

$$3^{1/2}(N/L)^{3/2} \leq a_0 \leq 1.35(N/L)\varepsilon^{-1/2}. \qquad (3.22)$$

Remark. In the derivation above, we have assumed that N is large. However for a constant feed rate $A(x) = 1$, this threshold is also valid for *any* N (without assuming that N is large). It corresponds to a zero-crossing of small eigenvalues [35], or equivalently, a bifurcation point for asymmetric spike solutions [36] of the system (1.1). Let us briefly summarize the latter computation here. Consider a steady state consisting of N equal interior spikes of (1.1). Such a steady state can be obtained using even reflections of a single interior spike on a domain $[-l, l]$,
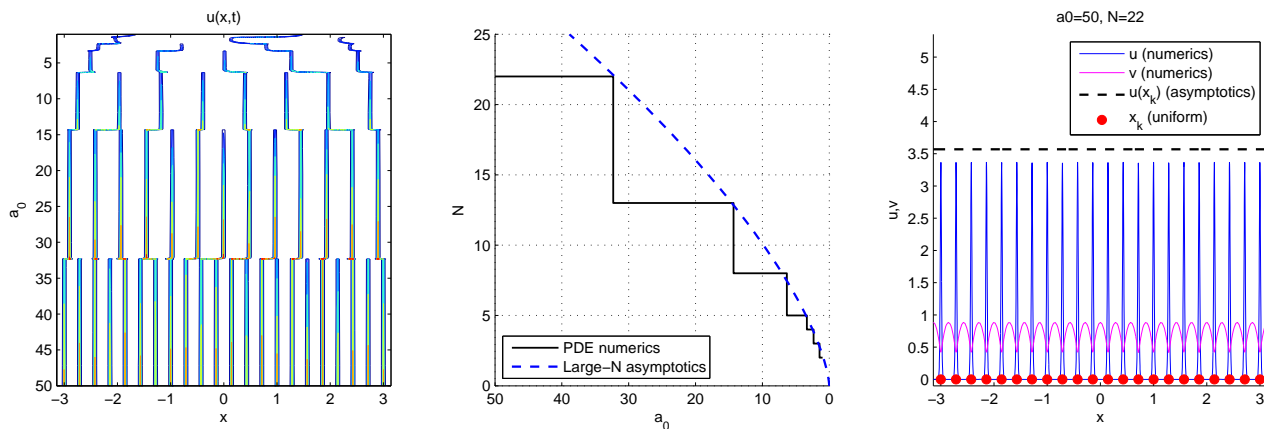
FIG. 3. Left: spike coarsening process with $A(x) = 1$. Other parameters are $\varepsilon = 0.007$ and $a_0 = 50 - 0.08t$. Middle: The number of spikes as a function of a_0. Solid stair curve corresponds to the observed number of spots from the numerical simulation. Dashed line is the theoretical prediction given by Main Result 2.2. Right: steady state consisting of 22 spikes.
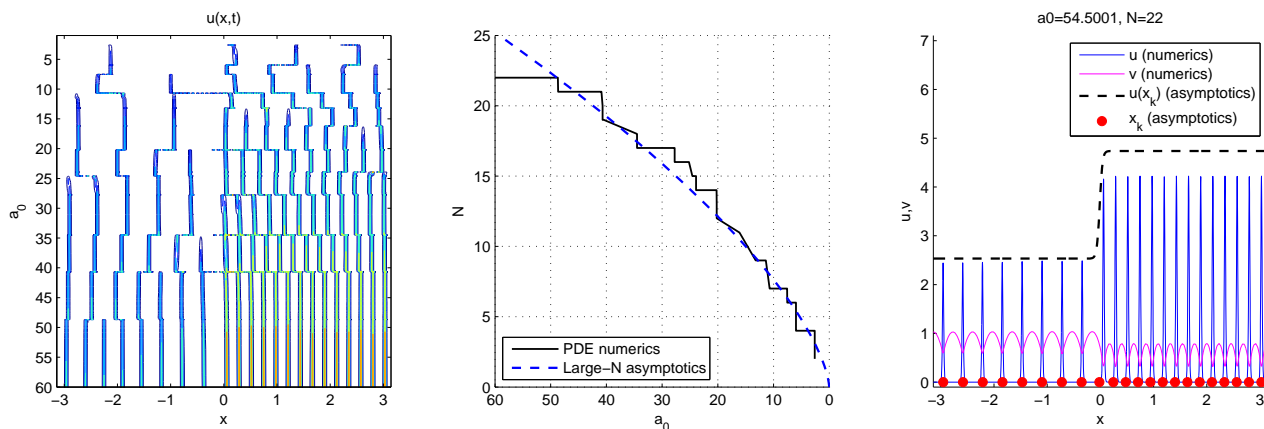

FIG. 4. Same as Figure 3 except that $A(x) = \begin{cases} 0.5, & x \in (-\pi, 0) \\ 1.5, & x \in (0, \pi) \end{cases}$.

where $l = L/N$. As in Appendix A, the asymptotic construction yields the outer solution of the form $v(x) \sim -a_0 \frac{x^2}{2} + l a_0 |x| + \frac{3}{a_0 l}$, $u(x) \sim \frac{a_0 l}{3} w(x/\varepsilon)$. Now define the function $f(l) = v(x)|_{x=l} = \frac{a_0 l^2}{2} + \frac{3}{a_0 l}$. This function has a minimum at $l^3 = 3/a_0^2$. Substituting $l = L/N$ and solving for a_0 yields precisely the left hand side of (3.22).

Figure 3 provides an illustration and a numerical verification of the lower bound of Proposition 3.2 (see caption). Excellent agreement is observed.

We now concentrate on the inhomogeneous case. As seen in the analysis of constant A, for a given constant C, and a given number A, there exists two solutions ρ of (2.17), as long as $C > 4b\left(1 - \log\left(4bA\right)\right)$; solution does not exist if inequality is reversed. But since $A = A(x)$ varies with x, we define

$$C_{\min} \equiv 4b\left(1 - \log\left(4b\min_{x \in [-L, L]} A(x)\right)\right). \tag{3.23a}$$

Also, define $M \equiv \int_{-L}^{L} \rho$. Then (3.23a) defines a curve $C(M)$ as a function of M. For $C > C_{\min}$, there are two admissable values of M. Unlike the case of constant A (where $M = 2L\rho$), not all positive values of M are admissable; a gap opens up – see Figure 2(right). The solution to (2.17), when exists, is the point along the curve $C(M)$ for which $M = 1$. As illustrated in Figure 2, there are two branches of the curve $C(M)$. The left branch is stable whereas the right branch is unstable. The disappearence of the steady state occurs when the $C = C_{\min}$. In other words, it is the solution to

$$\frac{A^2(x)}{\rho^3(x)} + 12b \log\left(\rho(x)/A(x)\right) = C_{\min} \tag{3.23b}$$
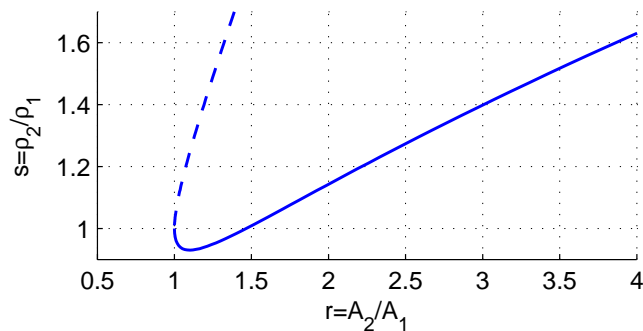
FIG. 5. The plot of (3.26).

where $\rho(x)$ is the smaller of the two admissable solutions, subject to the constraint

$$\int_{-L}^{L} \rho(x)dx = 1. \tag{3.23c}$$

We summarize this stability result as follows.

Proposition 3.3. *Let b be the solution to (3.23) and let $\alpha = (6/b)^{1/2}$. The N spike equilibrium becomes unstable resulting in spike death as a_0 is decreased below $N^{3/2}\alpha$.*

Interestingly, the competition thresholds for any N depends only on a single universal number α which must be computed from $A(x)$.

To illustrate Proposition 3.3, in Figure 1(d,e) we took $A(x) = 1 + 0.5\cos(x)$ with $L = \pi$. Numerical solution to (3.23) returns $\alpha = 0.504$ (compare this with $A(x) = 1, L = \pi$, $\alpha = 0.311$). Starting initially with $N = 22$ spikes and $a_0 = 65$, and very gradually decreasing a_0 as indicated in the Figure, As a_0 is decreased below $\alpha N^{3/2}$, the spikes start to dissapear one-by-one near the boundaries where $A(x)$ is at a minimum. This is in contrast to the case of constant $A(x) = 1$, for which about half of spikes are destroyed everytime the threshold is breached (see Figure 3). Figure 1(e) shows the curve $a_0 = \alpha N^{3/2}$ in excellent agreement with full numerics.

An important special case is when $A(x)$ is piecewise constant [29, 44]. Suppose that

$$A(x) = \begin{cases} A_1, & x \in I_1 \\ A_2, & x \in I_2 \end{cases} \quad \text{with } A_1 < A_2;$$

where the the domain $[-L, L]$ is a disjoint union of I_1, I_2 whose respective size is l_1, l_2 (so that $2L = l_1 + l_2$). A straightforward algebra yields the following solution to the system (3.23):

$$\frac{r^3}{s^3} = \exp\left(\frac{r^2}{s^3} - 1\right) \qquad \text{where } r = \frac{A_2}{A_1}; \quad s = \frac{\rho_2}{\rho_1}; \tag{3.24}$$

$$b = \frac{A_1^2}{4\rho_1^3}; \qquad \rho_1 l_1 + \rho_2 l_2 = 1. \tag{3.25}$$

The relationship (3.24) can be written in parametric form as

$$s = \frac{\exp\left(\frac{2}{3}(\tau - 1)\right)}{\tau}, \qquad r = \frac{\exp\left(\tau - 1\right)}{\tau} \tag{3.26}$$

and is plotted in Figure 5. Note that there are two branches that connect to $r = 1, s = 1$. The stable branch is indicated by a solid line.

For a concrete example, take $A_1 = 0.5$, $A_2 = 1.5$, $l_1 = l_2 = \pi$, so that $r = 3$ and from the graph in Figure 5, $s = 1.4 = \rho_2/\rho_1$. In particular, near the instability threshold, there are 1.4 as many spikes in the region where $A = 0.5$ than there are in the region where $A = 1.5$. From (3.25) we further obtain $b = 26.744$, $\alpha = 0.474$. Figure 4 shows excellent agreement with full numerics in this case.

Surprisingly, as seen in Figure 5, there is a narrow regime where the density of the spikes is *higher* in the areas of smaller feed. This occurs when $r = A_2/A_1 \in [1, 1.5]$.

Combining propositions 3.3 and 3.1 we now summarize our main finding as follows.

Main Result 3.4. *Suppose that $N\varepsilon \ll 1$. Then N spikes are stable when*

$$a_{0,coarse} < a_0 < a_{0,split} \tag{3.27}$$

where

$$a_{0,coarse} \equiv \alpha N^{3/2}; \qquad a_{0,split} \equiv \beta N \varepsilon^{-1/2}. \tag{3.28}$$

The constants α, β are given in Propositions 3.3 and 3.1, respectively. Coarsening (spike death) occurs when a_0 is decreased below $a_{0,coarse}$. Spike splitting occurs when a_0 is increased above $a_{0,split}$.

Equivalently, N spikes are stable provided that

$$N_{\min} < N < N_{\max} \tag{3.29a}$$

where

$$N_{\min} \equiv a_0 \frac{\varepsilon^{1/2}}{\beta}; \quad N_{\max} \equiv \left(\frac{a_0}{\alpha}\right)^{2/3} \tag{3.29b}$$

See Figure 1 and the introduction for illustration of this result and comparison with full numerics.

4. DISCUSSION

We used the Schnakenberg model with a space-dependent feed rate to illustrate how the dynamics of N interacting spots can be analysed by considering the large-N "mean-field" limit. For any fixed and finite N, the spot dynamics are controlled by a highly nonlinear, fully coupled differential-algebraic particle system for spot positions and their weights (2.4); this system is too complex to be tractable analytically (except in the case of constant feed rate, see [37, 45]). On the other hand, in the large-N limit we were able to fully characterize the resulting steady state as well as its stability. In this limit, the particle system is delicately balanced between the continuum and discrete worlds. This required a careful use of Euler-Maclaurin summation formula to estimate asymptotically the difference between various sums appearing in the particle system and their continuum (integral) approximations. Although we assumed that N is large in our derivation, the final results work very well even for relatively small N (e.g. $N = 4$), both for predicting the correct steady state as well as stability thresholds.

Using mean-limit approximations we found the upper and lower bounds for the number of stable spikes – see (3.29). The two bounds coincide when a_0 exceeds $a_{0,\max} \equiv \beta^3/\alpha^2 \varepsilon^{-3/2}$. For values of a_0 slightly above $a_{0,\max}$, complex creation-destruction loops can occur, provided that the feed rate $A(x)$ is "sufficiently inhomogeneous" (see Figure 1(f)). However when $A(x)$ is constant, no such loops occurs when $a_0 > a_{0,\max}$. Instead, the solution simply converges to a homogeneous state. Presumably, the destruction and creation of spikes must occur in different region, in order to produce complex creation-destruction loops, and this is not the case for a constant feed rate. Further investigation is needed to determine how "inhomogeneous" the feed rate $A(x)$ should be for such loops to exist. In any case, this provides for a nice demonstration that introducing space-dependence can lead to completely novel and complex dynamical phenomena that do not occur otherwise [28].

Until now, there are very few analytical results about large N limit in the literature. In two dimensions, a prominent example is the Gross-Pitaevskii Equation used to model Bose-Einstein condensates and whose solutions consist of vortex-like structures [4, 5]. For a two-dimensional trap, an asymptotic reduction for motion of vortex centers yields an interacting particle system [46–48], which in turn can be reformulated as a nonlocal PDE in the continuum limit of many vortices [23, 25]. While the analysis is quite different than the present paper, the end result is similar: one obtains instability thresholds which yields the maximum number of allowable vortices as a function of trap rotation rate and its chemical potential.

Numerous other PDE models have solutions that consist of N localized structures that interact in a nonlocal way, and we expect our techniques (with some modifications) to be applicable more widely to other reaction-diffusion systems such as Gray-Scott and Gierer-Meinhardt [28, 31], and more generally to other physical systems. The key takeaway message is that when the number of localized structures becomes large, a mean-field approach can yield important insights that cannot easily be obtained from looking at the finite N situation. We hope that the reader can attempt such approach on their own systems.

APPENDIX A: ODE'S FOR SPIKE CENTERS AND THE CORE PROBLEM

Here derive the reduced system for the motion of spike centers of the system (2.4), i.e. Proposition 2.1. The procedure is relatively standard. It consists of computing outer and inner solutions, using a solvability condition,

and matching. In the derivation below, we assume for simplicity that $A(x)$ is even although it generalizes easily to arbitrary $A(x)$.

Inner solution. Near k-th spike we expand:

$$u(x) = U(y), \quad v(x) = V(y), \quad y = \frac{x - x_k(t)}{\varepsilon}; \quad s = t$$

so that

$$-\varepsilon U_y x_k' = U_{yy} - U + U^2 V, \qquad 0 = V_{yy} + \varepsilon^2 a_0 A(x) - \varepsilon U^2 V.$$

Next expand

$$U = U_0 + \varepsilon U_1 + \dots, \quad V = V_0 + \varepsilon V_1 + \dots$$

At the leading order we obtain

$$0 = U_{0yy} - U_0 + U_0^2 V_0, \qquad 0 = V_{0yy}$$

It follows that

$$V_0(y) \sim V_0; \quad U_0(y) = w(y)/V_0$$

where $V_0 \sim v(x_k)$ will be obtained through inner-outer matching and $w(y)$ is the ground state satisfying

$$w_{yy} - w + w^2 = 0, \quad w'(0) = 0, \quad w(y) \to 0 \text{ as } y \to \pm\infty. \tag{4.30}$$

It is well known that the solution to (4.30) is given by by

$$w(y) = \frac{3}{2} \operatorname{sech}^2 (y/2). \tag{4.31}$$

The next order equations are

$$-x'(t) U_{0y} = U_{1yy} - U_1 + 2w U_1 + U_0^2 V_1 \tag{4.32}$$
$$V_{1yy} = U_0^2 V_0. \tag{4.33}$$

Multiply (4.32) by U_{0y} and integrate to obtain

$$-x'(t) \int U_{0y}^2 = \int U_0^2 U_{0y} V_1 = -\int \frac{U_0^3}{3} V_{1y} \tag{4.34}$$

Now

$$V_{1y} = \int_0^y U_0^2 V_0 dy + C$$

so that (4.34) becomes

$$x'(t) = C \frac{\int U_0^3}{3 \int U_{0y}^2} = C V_0 \frac{\int w^3}{3 \int w_y^2} \tag{4.35}$$

The constant C is determined as follows:

$$V_{1y}(+\infty) = \int_0^\infty U_0^2 V_0 dy + C; \quad V_{1y}(-\infty) = -\int_0^\infty U_0^2 V_0 dy + C;$$

$$C = \frac{V_{1y}(+\infty) + V_{1y}(-\infty)}{2}. \tag{4.36}$$

Outer expansion. Away from spike centers, $u(x)$ is assumed to be exponentially small so that $v_{xx} + a_0 A(x) = 0$ for $x \neq x_k$. Near x_k, the term $\frac{u^2 v}{\varepsilon}$ in (1.1) acts like a delta function so that we write

$$v_{xx} + a_0 A(x) \sim \sum_{j=1}^N s_j \delta (x - x_j). \tag{4.37}$$

Here, the weights s_j are defined by

$$s_k \equiv \int_{x_k^-}^{x_k^+} \frac{u^2 v}{\varepsilon} \sim \int_{-\infty}^{\infty} U_0^2 V_0 dy \sim \frac{1}{v_k} \int_{-\infty}^{\infty} w^2(y) dy \sim \frac{6}{v_k}$$

where we defined

$$v_k \equiv v(x_k).$$

The solution to (4.37) is then given by

$$v(x) = \sum_{j=1}^{N} s_j \frac{|x - x_j|}{2} - a_0 P(x) + mx + c$$

where m, c are constants to be determined and $P(x)$ is defined via

$$P''(x) = A(x); \quad P'(0) = 0.$$

For simplicity, we assume that $A(x)$ is even. In this case the constant m is zero as can be seen as follows. Compute $v'(\pm L)$ and set it to zero:

$$0 = v'(L) = \sum \frac{s_j}{2} - a_0 P'(L) + m,$$
$$0 = v'(-L) = -\sum \frac{s_j}{2} - a_0 P'(-L) + m.$$

Since P is even, $-P'(-L) = P'(L)$ so that $m = 0$. The expression for c is obtained by integrating (4.37) which yields

$$\int_{-L}^{L} a(x) = \sum s_j.$$

Finally, we also have $v(x_k) = v_k = 6/s_k$. We therefore obtain the following algebraic system for $s_k, k = 1 \ldots N$ and b:

$$\frac{6}{s_k} = \sum s_j \frac{|x - x_j|}{2} - a_0 P(x) + c, \quad k = 1 \ldots N; \tag{4.38a}$$

$$\sum s_j = a_0 \int_{-L}^{L} A(x) = 2a_0 P'(L). \tag{4.38b}$$

To compute $V_{1y}(\pm\infty)$, we match the inner and outer region. We have

$$V(y) \sim V_0 + \varepsilon V_1(y) \sim v(x_k + \varepsilon y) \sim v(x_k) + \varepsilon y v'(x_k^\pm)$$

so that

$$V_{1y}(\pm\infty) = v_x(x_k^\pm).$$

We further compute,

$$v(x_k^+) = \frac{s_k}{2} + \sum_{j \neq k} \frac{s_j}{2} \frac{x_k - x_j}{|x - x_j|} - a_0 P'(x_k)$$

$$v(x_k^+) = -\frac{s_k}{2} + \sum_{j \neq k} \frac{s_j}{2} \frac{x_k - x_j}{|x - x_j|} - a_0 P'(x_k)$$

so that the constant C in (4.36) evaluates to

$$C = \sum_{j \neq k} \frac{s_j}{2} \frac{x_k - x_j}{|x - x_j|} - a_0 P'(x_k). \tag{4.39}$$

Finally, we have

$$\int_{-\infty}^{\infty} w^2 dy = 6, \quad \int_{-\infty}^{\infty} w^3 dy = \frac{36}{5}, \quad \int_{-\infty}^{\infty} w_y^2 dy = \frac{6}{5},$$

so that (4.35) becomes

$$x_k'(t) = \frac{18}{s_k} \left(\sum_{j \neq k} \frac{s_j}{2} \frac{x_k - x_j}{|x - x_j|} - a_0 P'(x_k) \right) \tag{4.40}$$

subject to $N + 1$ algebraic constraints (4.38). Near x_k, the quasi-steady state is approximated by

$$u \sim w(y)/v_k, \quad v(x_k) \sim v_k, \quad v_k = \frac{6}{s_k}, \quad y = (x - x_k)/\varepsilon.$$

Equations (4.38a), (4.38b), and (4.40) are precisely the equations (2.4) in Proposition 2.1 after rescaling the spike weights and a_0 using the critical scaling

$$a_0 = (b/6)^{-1/2} N^{3/2}, \qquad s_j = (b/6)^{-1/2} N^{1/2} S_j. \tag{4.41}$$

Self-replication. Next we derive the self-replication thresholds. When s_k is too large, the inner problem becomes fully coupled. The relevant scaling for the inner problem in such a case is

$$u = \varepsilon^{-1/2} U, \ v = \varepsilon^{1/2} V, \quad x = x_j + \varepsilon y.$$

The leading-order inner problem for the steady state becomes

$$U_{yy} - U + U^2 V = 0, \quad V_{yy} - U^2 V = 0. \tag{4.42a}$$

We seek an even solution to (4.42a) subject to boundary conditions

$$U(y) \to 0 \text{ as } y \to \infty; \quad V_y(\infty) = B \text{ as } y \to \infty, \quad U'(0) = V'(0) = 0; \tag{4.42b}$$

where the constant B is related to the spike weight s_j as follows. Integrate the second equation in (4.42a) to obtain

$$2B = \int U^2 V dy = \varepsilon^{1/2} s_j. \tag{4.43}$$

The system (4.42) is referred to as the "core problem" and is used to explain the self-replication phenomenon such as shown in Figure 1(b). It was first identified in [38] in the context of the Gray-Scott model and was further studied in [39–43].

Numerical computations of the core problem (see for example [38, 39]) show that the solution to (4.42) exists only for

$$0 < B < B_c \approx 1.35.$$

As B is increased past B_c, the solution to the core problem dissapears as a result of a fold-point bifurcation. This dissapearence is responsible for the self-replication [39–42]. Substituting $B = B_c$ into (4.43), we see that the solution exists only if $s_j < 2.70\varepsilon^{-1/2}$. In terms of the rescaled weights S_j (4.41), this yields

$$S_j \le 2.70\varepsilon^{-1/2} \frac{N}{a_0}. \tag{4.44}$$

---

[1] S. Kondo, R. Asai, et al., A reaction-diffusion wave on the skin of the marine angelfish pomacanthus, Nature 376 (6543) (1995) 765–768.

[2] R. Barrio, C. Varea, J. Aragón, P. Maini, A two-dimensional numerical study of spatial pattern formation in interacting turing systems, Bulletin of mathematical biology 61 (3) (1999) 483–505.

[3] P. K. Maini, T. E. Woolley, R. E. Baker, E. A. Gaffney, S. S. Lee, Turing's model for biological pattern formation and the robustness problem, Interface focus (2012) rsfs20110113.

[4] J. Abo-Shaeer, C. Raman, J. Vogels, W. Ketterle, Observation of vortex lattices in bose-einstein condensates, Science 292 (5516) (2001) 476–479.

[5] M. H. Anderson, J. R. Ensher, M. R. Matthews, C. E. Wieman, E. A. Cornell, Observation of bose-einstein condensation in a dilute atomic vapor, science 269 (5221) (1995) 198–201.

[6] P. De Kepper, I. R. Epstein, K. Kustin, M. Orban, Systematic design of chemical oscillators. part 8. batch oscillations and spatial wave patterns in chlorite oscillating systems, The Journal of Physical Chemistry 86 (2) (1982) 170–171.

[7] Q. Ouyang, H. L. Swinney, Transition from a uniform state to hexagonal and striped turing patterns, Nature 352 (6336) (1991) 610–612.

[8] T. Kolokolnikov, M. Tlidi, Spot deformation and replication in the two-dimensional belousov-zhabotinski reaction in a water-in-oil microemulsion, Physical review letters 98 (18) (2007) 188303.

[9] M. B. Short, M. R. D'ORSOGNA, V. B. Pasour, G. E. Tita, P. J. Brantingham, A. L. Bertozzi, L. B. Chayes, A statistical model of criminal behavior, Mathematical Models and Methods in Applied Sciences 18 (supp01) (2008) 1249–1267.

[10] J. R. Zipkin, M. B. Short, A. L. Bertozzi, Cops on the dots in a mathematical model of urban crime and police response, to appear, DCDS-S (supplement).

[11] T. Kolokolnikov, M. J. Ward, J. Wei, The stability of steady-state hot-spot patterns for a reaction-diffusion model of urban crime., Discrete & Continuous Dynamical Systems-Series B 19 (5).

[12] S. Chaturapruek, J. Breslau, D. Yazdi, T. Kolokolnikov, S. G. McCalla, Crime modeling with lévy flights, SIAM Journal on Applied Mathematics 73 (4) (2013) 1703–1720.

[13] C. A. Klausmeier, Regular and irregular patterns in semiarid vegetation, Science 284 (5421) (1999) 1826–1828.

[14] J. A. Sherratt, An analysis of vegetation stripe formation in semi-arid landscapes, Journal of mathematical biology 51 (2) (2005) 183–197.

[15] J. A. Sherratt, G. J. Lord, Nonlinear dynamics and pattern bifurcations in a model for vegetation stripes in semi-arid environments, Theoretical population biology 71 (1) (2007) 1–11.

[16] Y. Chen, T. Kolokolnikov, J. Tzou, C. Gai, Patterned vegetation, tipping points, and the rate of climate change, European Journal of Applied Mathematics 26 (06) (2015) 945–958.

[17] L. P. Pitaevskii, S. Stringari, Bose-einstein condensation, no. 116, Oxford University Press, 2003.

[18] P. G. Kevrekidis, D. J. Frantzeskakis, R. Carretero-González, Emergent nonlinear phenomena in Bose-Einstein condensates: theory and experiment, Vol. 45, Springer Science & Business Media, 2007.

[19] M. C. Cross, P. C. Hohenberg, Pattern formation outside of equilibrium, Reviews of modern physics 65 (3) (1993) 851.

[20] J. D. Murray, Mathematical Biology. II Spatial Models and Biomedical Applications {Interdisciplinary Applied Mathematics V. 18}, Springer-Verlag New York Incorporated, 2001.

[21] J. Wei, M. Winter, Mathematical aspects of pattern formation in biological systems, Vol. 189, Springer Science & Business Media, 2013.

[22] F. Dalfovo, S. Giorgini, L. P. Pitaevskii, S. Stringari, Theory of bose-einstein condensation in trapped gases, Reviews of Modern Physics 71 (3) (1999) 463.

[23] D. E. Sheehy, L. Radzihovsky, Vortex lattice inhomogeneity in spatially inhomogeneous superfluids, Physical Review A 70 (5) (2004) 051602.

[24] A. Aftalion, X. Blanc, J. Dalibard, Vortex patterns in a fast rotating bose-einstein condensate, Physical Review A 71 (2) (2005) 023611.

[25] T. Kolokolnikov, P. Kevrekidis, R. Carretero-González, A tale of two distributions: from few to many vortices in quasi-two-dimensional bose–einstein condensates, in: Proc. R. Soc. A, Vol. 470, The Royal Society, 2014, p. 20140048.

[26] J. Murray, Why are there no 3-headed monsters? mathematical modeling in biology, Notices of the American Mathematical Society 59 (6) (2012) 785–795.

[27] R. G. Plaza, F. Sanchez-Garduno, P. Padilla, R. A. Barrio, P. K. Maini, The effect of growth and curvature on pattern formation, Journal of Dynamics and Differential Equations 16 (4) (2004) 1093–1121.

[28] K. M. Page, P. K. Maini, N. A. Monk, Complex pattern formation in reaction–diffusion systems with spatially varying parameters, Physica D: Nonlinear Phenomena 202 (1) (2005) 95–115.

[29] D. L. Benson, P. K. Maini, J. A. Sherratt, Unravelling the turing bifurcation using spatially varying diffusion coefficients, Journal of Mathematical Biology 37 (5) (1998) 381–417.

[30] A. Madzvamuse, A. J. Wathen, P. K. Maini, A moving grid finite element method applied to a model biological pattern generator, Journal of computational physics 190 (2) (2003) 478–500.

[31] J. Wei, M. Winter, Stable spike clusters for the one-dimensional Gierer-Meinhardt system, Submitted.

[32] K. Siteur, E. Siero, M. B. Eppinga, J. D. Rademacher, A. Doelman, M. Rietkerk, Beyond turing: The response of patterned ecosystems to environmental change, Ecological Complexity 20 (2014) 81–96.

[33] J. A. Sherratt, Using wavelength and slope to infer the historical origin of semiarid vegetation bands, Proceedings of the National Academy of Sciences 112 (14) (2015) 4202–4207.

[34] J. Schnakenberg, Simple chemical reaction systems with limit cycle behaviour, Journal of theoretical biology 81 (3) (1979) 389–400.

[35] D. Iron, J. Wei, M. Winter, Stability analysis of turing patterns generated by the schnakenberg model, Journal of mathematical biology 49 (4) (2004) 358–390.

[36] M. J. Ward, J. Wei, The existence and stability of asymmetric spike patterns for the schnakenberg model, Studies in Applied Mathematics 109 (3) (2002) 229–264.

[37] D. Iron, M. J. Ward, The dynamics of multispike solutions to the one-dimensional gierer–meinhardt model, SIAM Journal

on Applied Mathematics 62 (6) (2002) 1924–1951.

[38] J. E. Pearson, Complex patterns in a simple system, Science 261 (5118) (1993) 189–192.

[39] C. Muratov, V. Osipov, Spike autosolitons and pattern formation scenarios in the two-dimensional gray-scott model, The European Physical Journal B-Condensed Matter and Complex Systems 22 (2) (2001) 213–221.

[40] Y. Nishiura, D. Ueyama, A skeleton structure of self-replicating dynamics, Physica D: Nonlinear Phenomena 130 (1) (1999) 73–104.

[41] Y. Nishiura, D. Ueyama, Spatio-temporal chaos for the gray–scott model, Physica D: Nonlinear Phenomena 150 (3) (2001) 137–162.

[42] T. Kolokolnikov, M. J. Ward, J. Wei, The existence and stability of spike equilibria in the one-dimensional gray–scott model: the pulse-splitting regime, Physica D: Nonlinear Phenomena 202 (3) (2005) 258–293.

[43] T. Kolokolnikov, M. J. Ward, J. Wei, Spot self-replication and dynamics for the schnakenburg model in a two-dimensional domain, Journal of nonlinear science 19 (1) (2009) 1–56.

[44] D. L. Benson, J. A. Sherratt, P. K. Maini, Diffusion driven instability in an inhomogeneous domain, Bulletin of mathematical biology 55 (2) (1993) 365–384.

[45] D. Iron, M. J. Ward, J. Wei, The stability of spike solutions to the one-dimensional gierer–meinhardt model, Physica D: Nonlinear Phenomena 150 (1) (2001) 25–62.

[46] E. Weinan, Dynamics of vortex liquids in ginzburg-landau theories with applications to superconductivity, Physical Review B 50 (2) (1994) 1126.

[47] A. Aftalion, Q. Du, Vortices in a rotating bose-einstein condensate: Critical angular velocities and energy diagrams in the thomas-fermi regime, Physical Review A 64 (6) (2001) 063603.

[48] D. Yan, R. Carretero-González, D. Frantzeskakis, P. Kevrekidis, N. Proukakis, D. Spirn, Exploring vortex dynamics in the presence of dissipation: Analytical and numerical results, Physical Review A 89 (4) (2014) 043613.